Eur. Phys. J. A (2022) 58:169
https://doi.org/10.1140/epja/s10050-022-00793-9

THE EUROPEAN PHYSICAL JOURNAL A

Regular Article - Theoretical Physics

Triple high energy nuclear and hadron collisions - a new method to study QCD phase diagram at high baryonic densities

O. V. Vitiuk[1,2,3,4,a], **V. M. Pugatch**[4], **K. A. Bugaev**[2,5,b], **P. P. Panasiuk**[2], **N. S. Yakovenko**[2], **B. E. Grinyuk**[5], **E. S. Zherebtsova**[6,7], **M. Bleicher**[8], **L. V. Bravina**[3], **A. V. Taranenko**[6,7], **E. E. Zabrodin**[3,9]

[1] Institute of Theoretical Physics, University of Wroclaw, Max Born Pl. 9, 50-204 Wrocław, Poland
[2] Department of Physics, Taras Shevchenko National University of Kyiv, 03022 Kyiv, Ukraine
[3] University of Oslo, POB 1048, Blindern, 0316 Oslo, Norway
[4] Institute for Nuclear Research, National Academy of Sciences of Ukraine, Prospekt Nauki av. 47, 03680 Kyiv, Ukraine
[5] Bogolyubov Institute for Theoretical Physics, Metrologichna str. 14–B, Kyiv 03680, Ukraine
[6] National Research Nuclear University (MEPhI), Kashirskoe Shosse 31, 115409 Moscow, Russia
[7] Institute for Nuclear Research, Russian Academy of Science, 108840 Moscow, Russia
[8] Institute for Theoretical Physics, Goethe University, Max-von-Laue-Str. 1, 60438 Frankfurt am Main, Germany
[9] Skobeltsyn Institute of Nuclear Physics, Moscow State University, 119899 Moscow, Russia

Received: 1 June 2021 / Accepted: 15 July 2022 / Published online: 5 September 2022

Communicated by Evgeni Kolomeitsev

Abstract We propose an entirely new method to study the phase diagram of strongly interacting matter by means of scattering the two colliding beams at the fixed target. Here we present the results of simulations of the most central triple nuclear collisions with the UrQMD 3.4 model for the beam center-of-mass collision energies $\sqrt{s_{NN}} = 2.76$ TeV and $\sqrt{s_{NN}} = 200$ GeV. The main outcome of our modeling is that even at these very high collision energies the initial baryonic charge densities are about 3 times higher than the ones achieved in the ordinary binary nuclear collisions. As a result, for instance, the yields of protons and Λ-hyperons are strongly enhanced in the triple nuclear collisions. The other prospective applications of this method are briefly discussed. Among them we consider the low energy collisions of three nuclei of lead, passing through an intermediate system with an electric charge of 246 units which exceeds essentially the critical value of 173 and, hence, this may be of crucial importance to study the spontaneous emission of positron-electron pairs from the vacuum. We present the convincing arguments that the triple nuclear collisions method will allow the high energy nuclear physics community to create a new frontier in the studies of the QCD phase diagram and to lift up these studies to an entirely new level.

Supplementary Information The online version contains supplementary material available at https://doi.org/10.1140/epja/s10050-022-00793-9.

[a] e-mail: oleksandr.vitiuk@fys.uio.no (corresponding author)
[b] e-mail: bugaev@th.physik.unifrankfurt.de

1 Introduction

Investigation of the phase diagram of quantum chromodynamics (QCD) is the prime task of several ambitious experimental programs that are supplemented by rather sophisticated theoretical and numerical approaches. In the ongoing experiments on high energy nucleus-nucleus (A+A) collisions the center-of-mass energy of collisions ranges from $\sqrt{s_{NN}} = 2.42$ GeV (HADES), $\sqrt{s_{NN}} = 3.1$ GeV at RHIC BNL (Beam Energy Scan II) to $\sqrt{s_{NN}} = 17.3$ GeV at SPS CERN (NA61/SHINE) and further up to $\sqrt{s_{NN}} = 5.02$ TeV at the ALICE CERN. The major goals of these and completed experimental programs in the discussed collision energy range were to find the new state of matter, the quark-gluon plasma, to determine the collision energy thresholds of two phase transitions (PTs) expected to exist in QCD matter and to locate their (tri)critical endpoint(s). Unfortunately, after almost forty years of experimental studies of the QCD phase diagram nowadays we have only serious arguments that the quark-gluon plasma has, indeed, been created in A+A collisions, while two other goals are still far from being achieved [1][1].

[1] We apologize that here we cannot even mention many interesting results that are not directly related to the subject of this work.

Such a situation persists to exist due to objective reasons, the main of which are (I) the absence of PTs in a strict thermodynamic sense in A+A collisions due to the finite (or even small!) size of systems created in these reactions, (II) the inability of the lattice formulation of QCD to guide the experiments on A+A collisions and QCD phenomenology at high baryonic charge densities and (III) the lack of detailed experimental data measured with small steps in collision energy. Nevertheless, in our opinion under such hard circumstances, namely without a rigorous theory of phase transitions in finite systems, without clear and unambiguous signals of QCD PTs, the experimentalists and QCD phenomenologists did a great job and got some outstanding results and discoveries being more often guided by their enthusiasm and good luck rather than by the firm theoretical foundations. But the question is whether with the existing experimental methods and theoretical know-how the high energy nuclear physics (HENP) community will be able to accomplish its mission and to achieve the major goals during, let's say, a decade from now?

During the last 20 years, many promising theoretical results were obtained. But in our opinion on the theory side, the Functional Renormalization Group Method [2–4] and Dyson-Schwinger equations [5–7] provide the most coherent and consistent framework to study the QCD phase diagram. On the side of heavy ion collision phenomenology, two groups, using entirely different approaches to analyze the data, almost simultaneously came to similar conclusions: that the first order PT of (partial) chiral symmetry restoration to a phase of nearly massless hadrons occurs at the center-of-mass energies $\sqrt{s_{NN}} \simeq 4-5$ GeV [8–12], and that the deconfinement PT of color degrees of freedoms is either a very weak first-order PT or a second-order one with the threshold energy of A+A collisions being about $\sqrt{s_{NN}} \simeq 9-10$ GeV [8–12]. A conclusion that at finite values of baryonic chemical potential the chiral symmetry restoration PT occurs prior to the deconfinement one, i.e. at lower baryonic charge densities, obtained from the analysis of experimental data is in line with the well-known theoretical approaches [13–15].

However, the situation with the location of the (tri)critical endpoint is somewhat confusing yet [16,17], although the new estimates on its location made in Ref. [4] show that the situation is not hopeless. In fact, at present it is not even known for sure whether in QCD there exists a tricritical endpoint of these two PTs, or each PT has its own critical endpoint. Therefore, in order to accomplish its main mission, the HENP community has to do what it has not been done before. It is clear that on the theory side it is absolutely necessary to develop a rigorous theory of liquid-gas PTs in finite systems. Despite a limited progress achieved on a basis of the exact analytical solutions found for finite systems for a wide class of cluster models [18], the formulation of a rigorous theory of the liquid-gas PTs in finite systems is still in its infancy. The development of such an approach will move our experimental searches for the (tri)critical endpoint in A+A collisions to a solid ground.

On the experimental side, it is also necessary to get a reliable source of information about the equation of state of QCD matter which would be alternative and complementary to the A+A collision experiments. The importance of such an approach was understood recently and, hence, several groups independently suggested to employ the neutron stars and their coalescence to study the QCD matter equation of state at very high baryonic densities. Thus, neutron stars provide a possibility to test the region of the phase diagram from the vanishing temperature, typical for an equilibrated neutron star, up to around 70 MeV, reached during the neutron star mergers [19,20]. Moreover, the astrophysical observations, e.g. observations of two neutron stars with mass above $2M_\odot$ [21,22], simultaneous measurements of mass and radius of compact stars with NICER telescope [23,24], together with the tidal deformability limit obtained from the first binary neutron star merger GW170817 [25] have already constrained the equation of state at high density. Despite a big progress compact stars and on-ground A+A experiments so far can not probe the same part of the QCD phase diagram. As a step towards this direction the future experimental programs, i.e. NICA (JINR) [27] and FAIR (GSI) [26], are aimed to study the phase diagram of strongly interacting matter at highest baryon densities ever created in terrestrial laboratories.

In order to get an additional and independent information about the QCD matter equation of state at higher baryonic densities than the ones achieved in A+A collisions, here we suggest to perform the triple nuclear collisions (TNC) by bombarding the fixed target with two colliding beams. In this work, we mainly demonstrate the advantages of the TNC at very high collision energies of two beams $\sqrt{s_{NN}} = 200$ GeV (RHIC BNL) and $\sqrt{s_{NN}} = 2760$ GeV (LHC CERN), while some results for the low energies of collisions are also discussed.

The work is organized as follows. The next section is devoted to the analysis of TNC at LHC and the highest RHIC energies of collisions. In Sect. 3 we discuss new abilities and new challenges of the TNC method, while our conclusions are summarized in Sect. 4.

2 Modeling triple nuclear collisions by UrQMD 3.4

The idea to search for the TNC happening in the fixed solid target bombarded by two colliding beams was presented in 2018 at the Conference "CERN-Ukraine cooperation: current state and prospects" [28]. The TNC require two colliding beams and, hence, we are forced to study the high energy domain first, since the collider experiments at LHC CERN and RHIC BNL were designed to rather high collision ener-

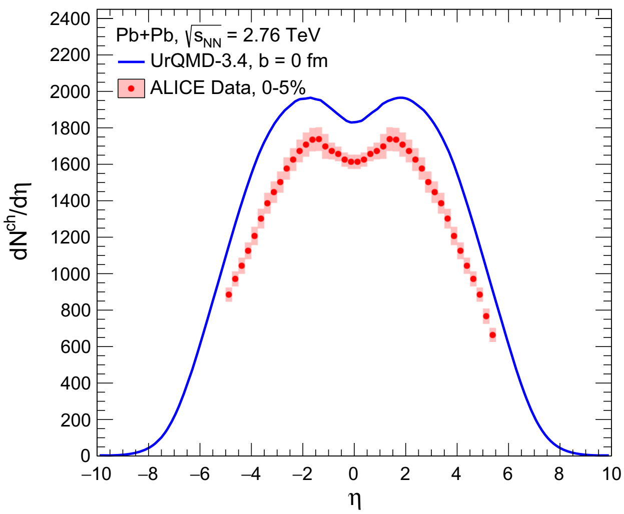

Fig. 1 Pseudorapidity distribution of charged particles $\frac{dN_{ch}}{d\eta}$ measured in 0–5% most central Pb+Pb collisions at $\sqrt{s_{NN}} = 2.76$ TeV (symbols) [37] vs. the UrQMD results (curve)

gies. Moreover, the possibility to use the LHCb-like detector for the fixed target experiments at LHC energies [29–31] and the STAR Fixed Target Program has been discussed already [32]. Now we suggest to extend this frame to employ it for investigating the TNC.

In order to demonstrate new opportunities of the TNC method to study the QCD phase diagram, we use the Ultra-relativistic Quantum Molecular Dynamics (UrQMD) transport model [33,34] (version 3.4) to simulate such collisions. For two decades the UrQMD [33,34] is successfully used to predict and describe the A+A collision experiments [35,36]. Although the UrQMD is widely used for RHIC BNL collision energies, its usage for A+A collisions at the LHC CERN energy $\sqrt{s_{NN}} = 2.76$ TeV should be made with some care [35]. Nevertheless, as shown in Ref. [37] the UrQMD is able to rather accurately describe the pseudorapidity distribution of charged particles $\frac{dN_{ch}}{d\eta}$ for the pseudorapidity values $|\eta| \leq 1$ and $|\eta| > 4$ for 0-5% and 5-10% of most central A+A collisions (see a discussion of Fig. 6 in [37]). Based on this result we studied the Pb+Pb collisions with a zero impact parameter $b = 0$ at $\sqrt{s_{NN}} = 2.76$ TeV using the UrQMD 3.4 to model the transport of hadrons and strings [33–35].

This setup is justified by the fact that in the present work we would like to compare the initial baryonic charge density and the bulk properties of hadron production achieved in the usual A+A collisions and in the TNC, while the analysis of phase transformations occurring during a collision process we reserve for the future explorations.

As one can see from Table 1 the UrQMD results for $b = 0$ found at midrapidity are very accurate for yields of protons, are within 2σ deviation for antiprotons and negative kaons, while for positive kaons they are less accurate. The largest deviation of about 30% one finds for the pions. In our opinion, this is rather good coincidence between the data and model, since we used a vanishing impact parameters, while the ALICE data correspond to the 0-5% bin of centrality class. Note also that the deviation of calculated hadronic yields from the measured ones should not create a problem, since this is a common feature of the A+A collisions and the TNC and, hence, there is a good hope that in the ratios of their spectra and their integrals such deviations will not play an important role or will be strongly reduced.

Figure 1 shows that the pseudorapidity distribution of charged particles at $|\eta| < 1$ is overestimated by the UrQMD by about 17%. Keeping these result in mind, we conclude that the UrQMD is able to reasonably well reproduce the bulk properties (amplitude and shape) of hadron

η distributions of the data measured in 0–5% most central Pb+Pb collisions at $\sqrt{s_{NN}} = 2.76$ TeV. The quality of A+A collision description at $\sqrt{s_{NN}} = 200$ GeV is similar [35]. Probably, one can improve the UrQMD setup to make a better agreement with the data. However, we strongly believe that such an accuracy is sufficient for the present work which aims to demonstrate to the HENP community the new abilities of the TNC method.

Now we turn to the TNC results (see Fig. 4 of Supplemental Materials for some examples and estimates for the TNC rate). Generally, simultaneous collision of three nuclei is almost impossible. In reality, the sequential TNC might happen, i.e. (A+A)+A and A+(A+A) collisions when one beam nucleus collides with a fixed target with a following creation of a fireball that interacts with the second beam nucleus after some time delay. To calculate the observables one should simulate sequential TNC with different time delays and then average over a delay time distribution. This effect should somehow smear particle distributions and reduce magnitudes of signals in comparison to the ideal TNC case. However, treatment of realistic cases is much more complicated and, hence, we leave this analysis for a future research. In this work, we will focus only on the absolutely central TNC with a simultaneous collision of two nuclei from beams with a target nucleus or, in the other words, the central simultaneous A+A+A events. Although, such collisions are idealized, apparently, they will provide an upper estimate of yields of secondary hadrons compared to the most central A+A collisions.

To adapt the UrQMD model for the simultaneous central TNC simulations we use two colliding nuclei with zero impact parameter. The initial distance between these nuclei is increased to be sufficient to fit the third nucleus between them. Afterwards the third nucleus, with the centre in the origin of coordinate system, was added between two colliding nuclei using standard UrQMD routine for nuclei initialization.

Table 1 Comparison of the ALICE CERN midrapidity hadronic yields measured in Pb+Pb collisions at $\sqrt{s_{NN}}$ = 2.76 TeV [38] with the results of UrQMD 3.4 output for the same energy

Data	π^+	π^-	K^+	K^-	p	$\bar{p}$
ALICE	669.5 ± 48	668 ± 47	100 ± 8	99.5 ± 8.51	31 ± 2.5	30.5 ± 2.5
UrQMD	933.7	934.5	121.6	117.4	31.7	26.5

It is clear that in the case of the central-simultaneous A+A+A reactions it is convenient to define the collision energy as the $\sqrt{s_{NN}}$ of two beam particles, but in the general case, it would be necessary to use the other notations in order to distinguish them from the A+A reactions. For the TNC of general type, it is more appropriate to introduce $\sqrt{s_{BB}^{beam}}$, i.e. the invariant mass of two colliding particles per pair of baryon charges. The double subscript BB here is introduced due to the fact, that for the sequential TNC the number of nucleons can be changed (melt) during the stage of A+A collision, but the baryonic charge is conserved.

The results of modeling the central-simultaneous TNC for the collision energy $\sqrt{s_{NN}} = 200$ GeV (highest RHIC energy) and $\sqrt{s_{NN}} = 2.76$ TeV (typical LHC energy) are shown in Figs. 2 and 3. As one can see from Fig. 2 the ratio of hadronic yields per rapidity unit expected for the TNC to the one for A+A collisions (3-to-2 nuclei enhancement factor hereafter), i.e. $R_{32}^{y} = \frac{dN_{AAA}}{dy} / \frac{dN_{AA}}{dy}$, are strongly increased for protons and for Λ-hyperons for the both values of collision energy analyzed here. For $\sqrt{s_{NN}} = 200$ GeV one can also see that at mid rapidity the yields of charged pions and positive kaons sizably enhanced, while for the LHC energy this effect for all mesons is very weak. These result show one that one possible way to detect the TNC collisions is to look for a simultaneous and enhanced yields of protons and Λ-hyperons.

In Fig. 3 we demonstrate the 3-to-2 nuclei enhancement factor of hadronic transversal momentum spectra in the TNC. Interestingly, there is an entirely different p_T behavior of this 3-to-2 nuclei enhancement factor at RHIC and LHC energies! At RHIC energy the momentum spectra of hadrons are enhanced by a p_T-independent factor (at least for $p_T < 2$ GeV). At the same time for the LHC energy of collisions, this scale factor is p_T-dependent and it decreases, if p_T increases. Moreover, as one can see from the lower panel of Fig. 3 the number of slow-moving mesons, i.e. the ones with $p_T < 0.4$ GeV is enhanced in the TNC compared to the A+A collisions, while the number of faster mesons is suppressed. In other words, it seems that the dense baryonic medium strongly decelerates the charged mesons at midrapidity or acts as a kind of density trap for mesons. This shows us that the hydrodynamic flow patterns expected at LHC energies in TNC may be highly nontrivial. Moreover, this figure shows that the effect is strongest for positive kaons and, hence, it

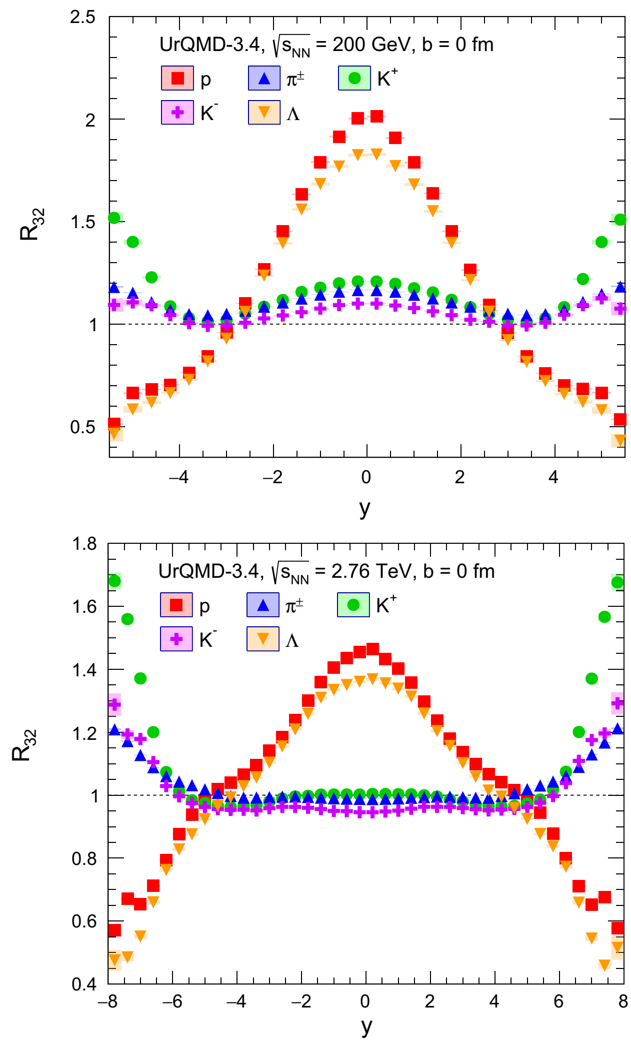

Fig. 2 **Upper panel:** The ratio of hadronic yields per rapidity unit $\frac{dN}{dy}$ expected for the TNC to the one for A+A collisions (3-to-2 nuclei enhancement factor) obtained for the same collision energy $\sqrt{s_{NN}} =$ 200 GeV as a function of particle rapidity. **Lower panel:** Same as in the upper panel, but for $\sqrt{s_{NN}} = 2.76$ TeV

is possible that at LHC energy one can expect an appearance of clusters of kaons or the droplets of kaonic matter. In this case, it is possible that in some events the clusters of mesonic matter can be sufficiently large to make a condensate. However, it is also possible that one has to take into account an enhanced number of slow-moving Λ-hyperons and, hence, one can alternatively expect not a mesonic con-

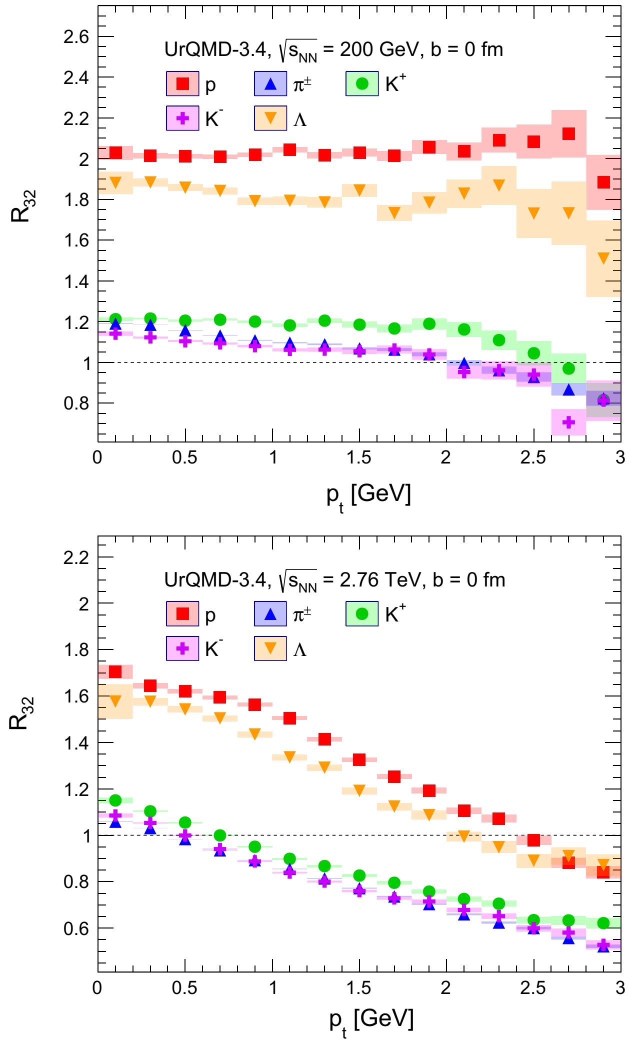

Fig. 3 **Upper panel:** Ratio of transversal momentum spectra of TNC to the one of A+A collisions (3-to-2 nuclei enhancement factor) of hadrons obtained for the same collision energy $\sqrt{s_{NN}} = 200$ GeV as a function of particle transverse momentum found at $|y| < 0.1$. **Lower panel:** Same as in the upper panel, but for $\sqrt{s_{NN}} = 2.76$ TeV

densate, but a formation of strange matter droplets or even the strangelets [40,41] We hope that the Hanbury-Brown–Twiss interferometry will be able to verify or disprove these hypotheses. Moreover, we believe that the conditions of the possible formation of dense and slow-moving strange matter in the TNC, i.e. appearance of density traps, should be studied further at higher and lower collision energies using more specialized transport models than the UrQMD. Perhaps, the 3-fluid hydro model [42] and its successor known as THESEUS [43] are the best candidates for such a study.

In Fig. 4 we show the time evolution of the baryonic charge density in the central cell of the volume 27 fm^3. We analyzed the range of cell volumes from 1 fm^3 to 27 fm^3 and found that for these values the results become volume independent for the central cell volume above 6 fm^3. Note that the time

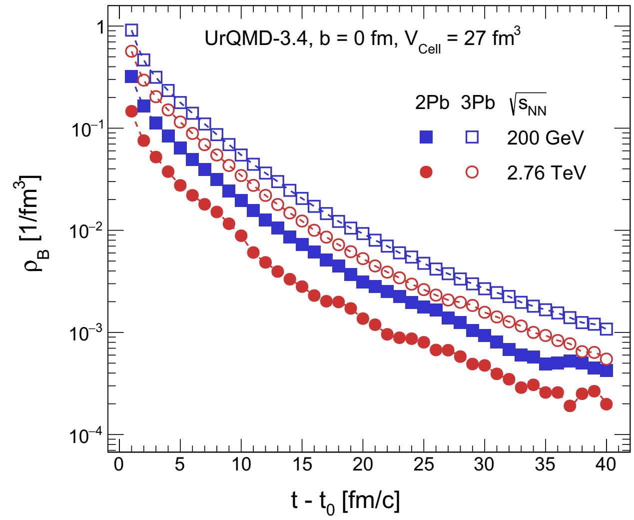

Fig. 4 Time evolution of baryonic charge density in the central cell having the volume 27 fm^3 during the course of A+A collisions (filled symbols) and the TNC (empty symbols) for $\sqrt{s_{NN}} = 200$ GeV (squares) and for $\sqrt{s_{NN}} = 2.76$ TeV (circles). The time t_0 is the moment at which the remnants of beam nuclei have passed through the central cell

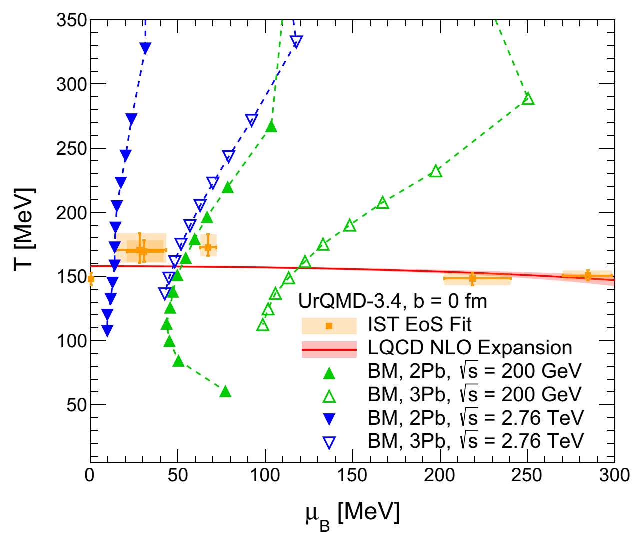

Fig. 5 Phase diagram in the $\mu_B - T$ plane and evolution of central cell parameters found with the help of MIT Bag Model [44]. The filled symbols correspond to A+A collisions, while the empty ones to the TNC. Collision energy $\sqrt{s_{NN}} = 200$ GeV corresponds to the triangles up, while the energy $\sqrt{s_{NN}} = 2.76$ TeV corresponds to the triangles down. The upmost points correspond to the time $t - t_0 > 1$ fm. The curve of pseudocritical temperature is given by a lattice QCD parameterization [47], while the crosses represent the parameters of chemical freeze-out in A+A collisions found in [48–50]. The collision energies of shown chemical freeze-out points of A+A collisions are (from left to right) $\sqrt{s_{NN}} = 2760, 200, 130, 62.4, 17.3, 12.3$ GeV [48–50]

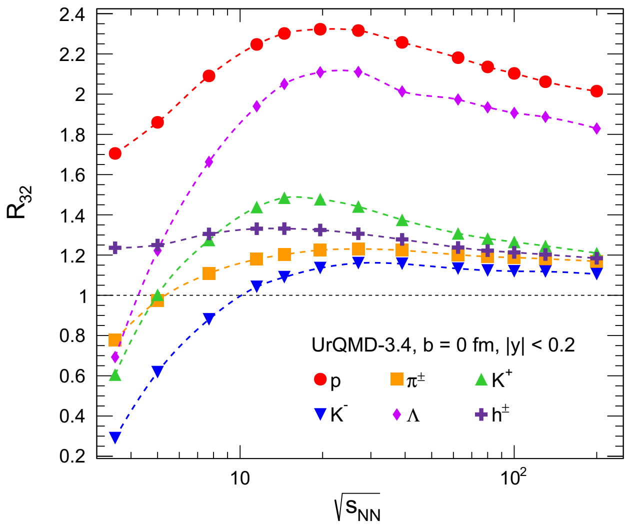

Fig. 6 3-to-2 nuclei enhancement factor of the hadronic yields for the central-simultaneous TNC $R_{32}^{y} = \frac{dN_{AAA}}{dy} / \frac{dN_{AA}}{dy}$ found at midrapidity as a function of $\sqrt{s_{NN}}$. The highest baryonic charge densities can be reached at $\sqrt{s_{NN}} \in [10; 40]$ GeV

$t_0 \simeq 10$ fm/c for the TNC and $t_0 \simeq 1$ fm/c for A+A collisions is the moment at which the remnants of beam nuclei have passed through the central cell. From Fig. 4 one can see a remarkable increase of the initial baryonic charge density in the TNC compared to the A+A collisions: from 0.321 to 0.913 fm^{-3} for $\sqrt{s_{NN}} = 200$ GeV and from 0.146 fm^{-3} to 0.567 fm^{-3} for $\sqrt{s_{NN}} = 2.76$ TeV. In other words, the initial baryonic charge density in the central cell in the case of TNC is about 3 times higher than for the A+A collisions. However, the energy density achieved in the TNC is practically the same as in the A+A collisions.

To quantify the increase of baryonic chemical potential achieved in the TNC we employ the MIT Bag Model equation of state (EoS) [44] for 3 quark flavors and 3 colors. For massless quarks, its pressure as the function of system temperature T and baryonic chemical potential μ_B can be written as

$$p^{BM} = \frac{95}{180}\pi^2 T^4 + \frac{T^2 \mu_B^2}{6} + \frac{\mu_B^4}{108\,\pi^2} - B_{vac}\,, \tag{1}$$

where the vacuum pressure B_{vac} was chosen as $B_{vac}^{\frac{1}{4}} = 206$ MeV [45]. This value of B_{vac} is a conservative estimate which is widely accepted [46].

From the pressure (1) one can find the baryonic charge density ρ_B, entropy density s, and energy density ϵ using the thermodynamic identities

$$\rho_B^{BM} = \frac{\partial p^{BM}}{\partial \mu_B}\,, \quad s^{BM} = \frac{\partial p^{BM}}{\partial T}\,, \tag{2}$$

$$\epsilon^{BM} = T s^{BM} + \mu_B\, \rho_B^{BM} - p^{BM}\,. \tag{3}$$

Equating ρ_B^{BM} and ϵ^{BM} to the quantities found in central cell for the TNC, one can find $T(t)$ and $\mu_B(t)$ at different times t of evolution. The results for $T(t)$ and $\mu_B(t)$ are shown in Fig. 5 both for the TNC (empty symbols) and for the A+A collisions (filled symbols). In Fig. 5 we demonstrate all solutions found by this procedure, but it is apparent that one cannot trust them below the pseudocritical curve (solid curve in Fig. 5) taken from the recent lattice QCD work [47].

For the sake of comparison, in Fig. 5 we show also the parameters of chemical freeze-out in A+A central collisions found by the most advanced version of the hadron resonances gas model based on the induced surface tension EoS [48–50]. Within the induced surface tension approach these parameters for the collision energy $\sqrt{s_{NN}} = 2.76$ TeV were first found in Ref. [48], while the points for $\sqrt{s_{NN}} =$ 200, 130, 62.4, 17.3, 12.3 GeV were reported in Ref. [49]. The found parameters of chemical freeze-out for $\sqrt{s_{NN}} =$ 200 GeV and $\sqrt{s_{NN}} = 2.76$ TeV were recently confirmed in Ref. [50] within the most sophisticated formulation of the hadron resonances gas model.

The chemical freeze-out points demonstrate to us the accuracy of the MIT Bag Model predictions for the baryonic chemical potential: from the results of Refs. [48–50] it is known that at chemical freeze-out curve for the collision energy $\sqrt{s_{NN}} = 2.76$ TeV the baryonic chemical potential is $\mu_B^{CFO} \leq 1$ MeV at $T^{CFO} \simeq 148 \pm 2$ MeV [50], while for the collision energy $\sqrt{s_{NN}} = 200$ GeV the chemical freeze-out parameters should be $\mu_B^{CFO} \simeq 30 \pm 3.25$ MeV for $T^{CFO} \simeq 167.3 \pm 3.9$ MeV [50]. Comparing these numbers with the evolutionary trajectories shown in Fig. 5, one can conclude that near the chemical freeze-out our estimates based on the conservative MIT Bag Model parameterization [45,46] provide an accuracy of about 13 MeV for μ_B^{CFO} for A+A reactions at $\sqrt{s_{NN}} = 2.76$ TeV and the one of about 27 MeV for such reactions at $\sqrt{s_{NN}} = 200$ GeV. In our opinion these are quite reasonable estimates keeping in mind the simplicity of the MIT Bag Model and several assumptions adopted here.

Although the main purpose of Fig. 5 is to quantify the increase of baryonic chemical potentials achieved in the course of TNC compared to the A+A collisions, we would like also to point out a peculiar property, which may be a pure coincidence. From Fig. 5 one can see that the evolutionary trajectory of the central cell in the TNC at $\sqrt{s_{NN}} = 2.76$ TeV is very close to the one found at $\sqrt{s_{NN}} = 200$ GeV in the A+A collisions. This feature should be investigated further with more realistic transport models, since comparison of two almost identical systems existing at a central cell which, nevertheless, have rather different flow patterns outside this cell (just compare the panels of Figs. 2 and 3) may open a unique opportunity to study the QCD matter EoS under the different evolution conditions.

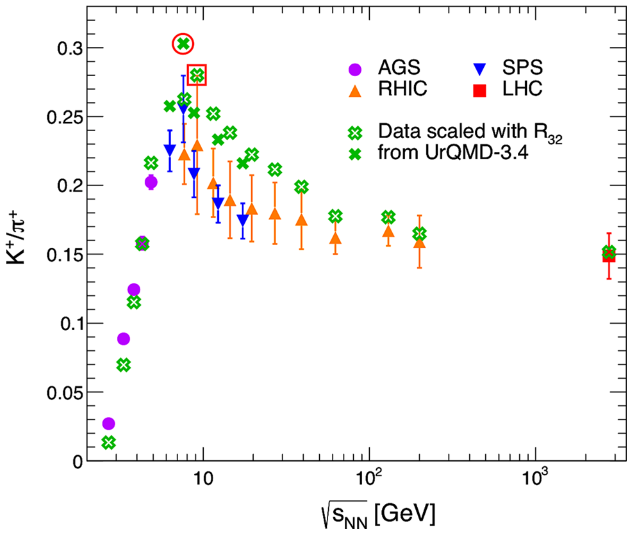

Fig. 7 Prediction for the $\sqrt{s_{NN}}$ dependence of the $\frac{K^+}{\pi^+}|_{AAA}$ ratio for the central-simultaneous TNC based on existing data from E866/E917 [52], NA49 [53,54], STAR [55–57] and ALICE [38] collaborations. Scaled SPS data are represented by filled crosses when scaled AGS, RHIC, and LHC data are represented by empty symbols. The found maxima are discussed in the text

It is easy to see that for the Bag Model pressure (1) the equation of isentropic expansion $s^{BM}/\rho_B^{BM} = const$ is equivalent to the condition $\mu_B/T = const$. Inspecting Fig. 5, one can see that at the moment of crossing the pseudocritical curve [47] the trajectory of the central cell evolution is very close to the condition $\mu_B/T = const$, i.e. to an isentropic expansion. Apparently, this feature of the TNC should be also studied in more detail along with the mechanisms of entropy generation in such collisions.

Also, we want to mention that with the TNC method one can vary μ_B only changing the central nucleus at constant collision energy. This could lead us to the new method of study QCD phase diagram with at different μ_B but almost constant T values.

3 New abilities and new challenges of the TNC

In the preceding section, we discussed the new opportunities of the TNC method at very high collision energies. Keeping, however, in mind the fact that the RHIC can, in principle, operate in a colliding mode of two nuclei at lower energies and that the NICA accelerator at JINR [51] is a low energy collider as well, in Fig. 6 we summarize the collision energy dependence of the 3-to-2 nuclei enhancement factor for the central-simultaneous TNC. From this figure, one can deduce that, most probably, the effects of proton, Λ-hyperon and positive kaon production will be even stronger at $\sqrt{s_{NN}} \in [10; 40]$ GeV. According to the results of Refs. [8–12] this is a region just above the A+A collision energy threshold of the deconfinement PT. Due to the importance of this energy range, we prepared the predictions for the $\frac{K^+}{\pi^+}|_{AAA}$ ratio collision energy dependence which is expected in the TNC. Using the 3-to-2 nuclei enhancement factors shown in Fig. 6 and the well-known experimental data for $\frac{K^+}{\pi^+}|_{AA}$ ratio measured in the A+A collisions, we constructed Fig. 7 according to the formula $\frac{K^+}{\pi^+}|_{AAA} = \frac{K^+}{\pi^+}|_{AA} \cdot R_{32}^{K+}/R_{32}^{\pi+}$.

The main question that puzzles one is that the SPS and RHIC data extrapolation to the TNC lead to the different location of the $\frac{K^+}{\pi^+}|_{AAA}$ peak (see Fig. 7). This figure also demonstrates the crucial importance to have accurate experimental data for analysis and for reliable theoretical predictions. The point is that according to Refs. [8–12] the location of $\frac{K^+}{\pi^+}|_{AAA}$ peak, either at $\sqrt{s_{NN}} = 7.7$ GeV (prediction based on SPS data, shown by a cross inside the circle in Fig. 7) or at $\sqrt{s_{NN}} = 9.2$ GeV (prediction based on RHIC data, shown by a cross inside the square in Fig. 7), can lead to entirely different interpretations of the physics case: either the mass of strange quark carrier starts to change at 7.7 GeV, i.e. after the chiral symmetry restoration PT in hadronic phase and before the deconfinement, or the peak at 9.2 GeV can be considered as a new signal of deconfinement PT, or there may exist two peaks of this ratio. Hence, it would be important to measure this ratio in the TNC in order to find out an exact location of its peak, to verify our prediction, and to determine what set of A+A data, either SPS data or RHIC ones, is compatible with the TNC results. The existing theoretical models for the EoS of dense QCD phases can also make their predictions for the outcome of the TNC prior to the experiments. Then after experiments, the HENP community can easily see what EoS is the most realistic one.

It is clear that the TNC method not only opens new research opportunities, but at the same time it creates new challenges for the whole row of hot topics discussed presently by the HENP community. Among the most prospective hot topics, we can name the jet tomography [58,59] in a dense and quark rich medium (compared to A+A collisions) created in the TNC, the chiral magnetic effect [60], and the chiral vortical effect [61,62] for the non-central TNC. Also, the non-central TNC may shed a new light on the polarization phenomenon of (anti)Λ-hyperons [63,64] inside the baryonic charge rich medium. At this stage of research, one can only guess about the outcome of the TNC method for resolving the puzzles of formation of nuclear clusters in nuclear collisions recently discussed in [50,65–72].

Among the other challenges, it is necessary to mention the numerical modeling of the TNC by the other transport models and by the hydrodynamic ones. Our educated guess is that at low collision energies the TNC will finally require to use the correct cut-off formula [73] for the emission of secondary particles which, in contrast to the approximative Cooper-Frye formula, does not have the contributions of negative number of particles. Moreover, in this case for reliable modeling of the TNC at low collision energies, it will be also necessary to reformulate the equations of relativistic hydrodynamics and hydro-kinetics according to the correct equations of energy-momentum and charge conservations [75,76] which are mathematically consistent with the boundary (kinetic freeze-out) conditions. Besides, an experimental detection and theoretical modeling of the elliptic, triangular and higher order flow patterns [77,78] for the TNC may be another challenge for the HENP community.

We believe that the TNC method can help to ultimately resolve the problem of creating the systems with electric charges Q which are essentially larger than the critical one $Z_{cr} \simeq +173$ units of elementary charge e in heavy ion collisions. This problems has an extended history [79], but with somewhat unclear output. Due to its fundamental aspects, namely the creation of an unstable vacuum and spontaneous emission of positron-electron pairs from it, this problem still attracts a high attention of theoreticians [80]. The TNC method has some advantages over the other ones, since the total electric charge of three lead nuclei is $Z_{PbPbPb} = 246$, i.e. it is about 34% larger than the electric charge of two colliding uranium nuclei $Z_{UU} = 184$. Moreover, the effects of Lorentz contraction of two colliding nuclei can essentially increase the electric field even for not very relativistic energies. This gives us a hope that in the TNC the spontaneous emission of positron-electron pairs can be essentially higher and, hence, the ratio of signal to the background, in this case, can be more favorable than in the A+A collisions.

Ab initio simulations of the electromagnetic field created in the A+A collision is a very complicated task [81]. Therefore, for the TNC we made a simplified model and compared it with the results obtained from the instantaneous nucleon density distributions found from the UrQMD 3.4 simulations.

In Fig. 8 we demonstrate the evolution of the apparent charge

$$\frac{Q_{app}(y,t)}{Z_{cr}e} = \frac{4\pi E_y(y)}{Z_{cr}e} y^2 \,, \text{ for } y \geq R_{Pb} \,, \tag{4}$$

seeing at the time t on the distance $|y|$ along the $\mathbf{y}$-axis which is perpendicular to the beam axis $\mathbf{z}$. Here R_{Pb} denotes the radius of the lead nucleus. The center of the coordinate system is located at the geometrical center of the target nucleus. The y-component of the electric field strength $E_y(y,t)$ in the TNC was found from the velocity and spacial distributions of electric charges by the UrQMD. Knowing these distributions one can calculate the electric field strength $E_y(y,t)$ and the apparent charge (4). A simple analytical model (its results are shown in Fig. 8 by the short dashed curve) is presented in the Supplementary Materials. It is used to a quick extrapolation of the UrQMD results for the Q_{app} to later times in order to save the CPU time. Also, it provides a simple analytical parameterization, which we found to be reasonably good.

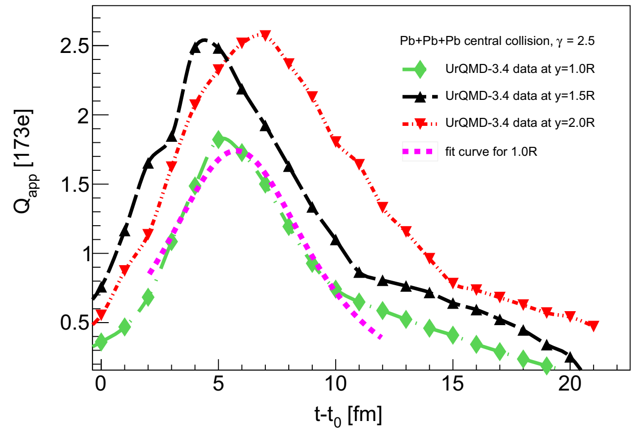

Fig. 8 Time evolution of the apparent charge Q_{app} given in the units of the critical one on the distance $|y|$ from the center of the target Pb nucleus. The γ-factor of beam nuclei is 2.5 in the rest frame of target nucleus. The results obtained from the UrQMD simulations are shown for $|y| = R_{Pb}$, $1.5R_{Pb}$ and $2R_{Pb}$. Here the initial time $t - t_0 = 0$ is the moment, when two colliding nuclei have passed through the central nucleus and start to interact with each other. The maximum of Q_{app} corresponds to a moment, when the remnants of nuclei have passed through each other. For more details see the Supplementary Materials

From the time dependence of Q_{app} shown in Fig. 8 one can see that during the course of the TNC the apparent charge increases to a maximal value which for the γ-factor of projectile nuclei being $\gamma = 2.5$ can be as large as $\max\left[Q_{app}(|y| = 2R_{Pb}, t)\right] \simeq 2.5\, Z_{cr}\, e \simeq 432.5e$! This is an enormous increase compared to the A+A collisions. Moreover, in contrast to the ordinary static case in the TNC, the charge $Q_{app}(y,t)$ increases with the distance from the center of the target nucleus. This means that a strong electric field can produce the positron-electron pairs in a larger volume which, hopefully, may lead to a stronger emission of such pairs. Actually, if this is the case and the number of spontaneously emitted pairs is large, we suggest to use the methods of Hanbury-Brown–Twiss interferometry to these pairs and to study the positron-positron, positron-electron, or electron-electron correlations in order to find out the space-time picture of their emission process in the TNC. Apparently, the collisions of three uranium nuclei with the total electric charge of 276 elementary ones would be even more interesting.

Above we considered one extreme, namely the triple collisions of heavy atomic nuclei, but it is clear that the other extreme, i.e. the triple collisions of stable hadrons ($p+p+p$ or $p+n+p$ or even $p+p+\bar{p}$ ect) are also possible to perform. Of course, the proton target, i.e. gaseous hydrogen, can be easily made, while for the neutron target one better uses the deuterium target. Since the protons are composite objects their triple, but sequential collisions can give us a unique opportunity to study the interaction of partonic medium created in a collision of two protons with the third colliding proton. This may help us to find out the new features of the many-parton distribution functions inside the proton in the new regime. This is another hot topic of modern high energy physics discussed recently in [82].

Also, it would be interesting to exploit the fixed target regime in the electron-positron colliders. Lepton colliders collide fundamental particles, hence the initial state of each event is known, and, moreover, compared to hadronic colliders, the measurements with higher precision can be achieved. Using the existing electron-positron colliders and the new ones, like the Compact Linear Collider (CLIC), it will be possible to study the interaction of products of electron-positron collisions with nuclei of a target. The other applications of the TNC method are briefly discussed in the Supplemental Materials.

4 Conclusions and perspectives

In this work, we gave convincing arguments that the TNC method will allow the HENP community to create a new frontier in the studies of the QCD phase diagram. This new frontier will make a strategic change in the present situation from the status "still hard to win" to the status "success guaranteed". Our conclusion is based on a result that a strong enhancement of baryon yields in the TNC is found. Predictions for enhancement factors are made for various current and future collider's experiments. Some new features of electron-positron pair production in the TNC are underlined.

However, it is clear that the detection of TNC is highly non-trivial and seems unattainable at the current stage of technology development. Nevertheless, in this article, we propose the theoretical concept of this new method for studying the properties of QCD matter.

Acknowledgements Discussions with D.B. Blaschke, V. Yu. Denisov, F. Fleuert, G. Grazziani, G. Manca, S. N. Nedelko, E. G. Nikonov, P. Robbe, M. Schmelling, Ivan P. Yakimenko, D. L. Borisyuk, O. Ivanytskyi, V. Sagun and with all members of the LHCb IFT WG are highly appreciated. K.A.B. acknowledges a support from the NAS of Ukraine by its priority project "Fundamental properties of the matter in the relativistic collisions of nuclei and in the early Universe" (No. 0120U100935). The work of L.V.B. and E.E.Z. was supported by the Norwegian Research Council under grant No. 255253/ F53, and by the RFBR grants 18-02-40085 and 18-02-40084. E.S.Zh., K.A.B., O.V.V. and L.V.B. thank the Norwegian Agency for International Cooperation for the support under grants CPEA-LT-2016/10094 and UTF-2016-long-term/10076. A.V.T. acknowledges partial support from RFBR under grant No. 18-02-40086 and from the Ministry of Science and Higher Education of the Russian Federation, Project No 0723-2020-0041. V.M.P. acknowledges a support from the NAS of Ukraine Programs to enhance a cooperation with CERN and JINR "Fundamental research on high-energy physics and nuclear physics", and a partial support from LIA IDEATE (STCU grant within the Project P9903). The simulations were done on the JINR supercomputer Govorun.

Data Availability Statement This manuscript has data included as electronic supplementary material. The online version of this article contains supplementary material, which is available to authorized users.

References

1. J. Adolfsson et al., Eur. Phys. J. A **56**(11), 288 (2020)
2. J.M. Pawlowski, Ann. Phys. **322**, 2831–2915 (2007)
3. B.-J. Schaefer, J. Wambach, Phys. Part. Nucl. **39**, 1025–1032 (2008)
4. F. Gao, J.M. Pawlowski, Phys. Rev. D **102**, 034027 (2020)
5. R. Alkofer, L. von Smekal, Phys. Rept. **353**, 281 (2001)
6. C.S. Fischer, J. Phys. G **32**, R253 (2006)
7. G. Eichmann, H. Sanchis-Alepuz, R. Williams, R. Alkofer, C.S. Fischer, Prog. Part. Nucl. Phys. **91**, 1–100 (2016)
8. K.A. Bugaev et al., Phys. Part. Nucl. Lett. **12**, 238–245 (2015)
9. K.A. Bugaev et al., Eur. Phys. J. A **52**, 175–189 (2016)
10. W. Cassing, A. Palmese, P. Moreau, E.L. Bratkovskaya, Phys. Rev. C **93**, 014902 (2016)
11. A. Palmese et al., Phys. Rev. C **94**, 044912 (2016)
12. K.A. Bugaev et al., Phys. Part. Nucl. Lett. **15**, 210–224 (2018)
13. Y. Nambu, G. Jona-Lasinio, Phys. Rev. **122**, 345 (1961)
14. S.P. Klevansky, Rev. Mod. Phys. **64**, 649 (1992)
15. L. McLerran, R.D. Pisarski, Nucl. Phys. A **796**, 83 (2007)
16. F. Rennecke, MDPI Proc. **10**, 8 (2019)
17. STAR Collaboration (M.M. Aggarwal et al.,), arXiv:1007.2613 [nucl-ex] (2010)
18. K.A. Bugaev, P.T. Reuter, Ukr. J. Phys. **52**, 489–510 (2007). [arXiv:1001.4477 [nucl-th]]
19. A. Bauswein et al., Acta Phys. Polon. B **51**, 551 (2020)
20. E.R. Most et al., Phys. Rev. Lett. **122**, 061101 (2019)
21. J. Antoniadis et al., Science **340**, 1233232 (2013)
22. H.T. Cromartie et al., Nature Astr. **4**, 72 (2020)
23. T.E. Riley et al., Astroph. J. Lett. **918**, L27 (2021)
24. M.C. Miller et al., Astroph. J. Lett. **918**, L28 (2021)
25. LIGO/Virgo Scientific Collaborations (B.P. Abbott et al.,) Phys. Rev. Lett. **119**, 161101 (2017)
26. Proceedings of the (FAIRNESS 2019) (Edited by M. Destefanis et al.,) J. Phys. Conf. Ser. **1667**, 1 (2020)
27. D. Blaschke et al., Topical issue on exploring strongly interacting matter at high densities - NICA white paper. Eur. Phys. J. A **52**, 267 (2016)
28. V. Pugatch, Physics and techniques of the fixed metal microstrip target for the LHCb experiment, talk at the Int. Conference CERN-Ukraine cooperation: current state and prospects, Kharkiv. 15 of May (2018). https://cds.cern.ch/record/2658000
29. L. Massacrier et al., Adv. High Energy Phys. **2015**, 986348 (2015)
30. L. Massacrier et al., Int. J. Mod. Phys. Conf. Ser. **40**, 1660107 (2016)
31. V. Pugatch, Ukr. J. Phys. **64**(7), 619 (2019)

32. K.C. Meehan (for the STAR Collaboration), Nucl. Phys. A **956**, 878–881 (2016)
33. S.A. Bass et al., Prog. Part. Nucl. Phys. **41**, 225–370 (1998)
34. M. Bleicher et al., J. Phys. G **25**, 1859–1896 (1999)
35. H. Petersen, J. Steinheimer, G. Burau, M. Bleicher, H. Stöcker, Phys. Rev. C **78**, 044901 (2008)
36. S. Sombun et al., Phys. Rev. C **99**, 014901 (2019)
37. ALICE Collaboration, Phys. Lett. B **726**, 610–622 (2013)
38. ALICE Collaboration (B. Abelev et al.), Phys. Rev. C **88**, 044910 (2013)
39. ALICE Collaboration (J. Adam et al.), Phys. Rev. C **93**, 034913 (2016)
40. A.R. Bodmer, Phys. Rev. D **4**, 1601–1606 (1971)
41. E. Witten, Phys. Rev. D. **30**, 272–285 (1984)
42. Y.B. Ivanov, A.A. Soldatov, Phys. Rev. C **97**(2), 024908 (2018)
43. P. Batyuk et al., EPJ Web Conf. **182**, 02056 (2018)
44. A. Chodos, R.L. Jaffe, K. Johnson, C.B. Thorn, V.F. Weisskopf, Phys. Rev. D **9**, 3471 (1974)
45. C.Y. Wong, *Introduction to High-Energy Heavy Ion Collisions* (World Scientific, Singapore, 1994), p.516
46. W. Florkowski, *Phenomenology of Ultra-Relativistic Heavv-Ion Collisions* (World Scientific, Singapore, 2010), p.416
47. S. Borsanyi et al., Phys. Rev. Lett. **125**, 052001 (2020)
48. K.A. Bugaev et al., Nucl. Phys. A **970**, 133–155 (2018)
49. V.V. Sagun et al., Eur. Phys. J. A **54**, 6–100 (2018)
50. K.A. Bugaev et al., Eur. Phys. J. A **56**, 293 (2020)
51. For the latest news on the Megaproject NICA see https://nica.jinr.ru (2020)
52. E866 Collaboration (L. Ahle et al.), Phys. Lett. B **476**, 1–8 (2000)
53. NA49 Collaboration (S.V. Afanasiev et al.), Phys. Rev. C **66**, 054902 (2002)
54. NA49 Collaboration (C. Alt et al.), Phys. Rev. C **77**, 024903 (2008)
55. STAR Collaboration (B.I. Abelev et al.), Phys. Rev. C **79**, 034909 (2009)
56. STAR Collaboration (B.I. Abelev et al.), Phys. Rev. C **81**, 024911 (2010)
57. STAR Collaboration (L. Adamczyk et al.), Phys. Rev. C **96**, 044904 (2017)
58. X.N. Wang, M. Gyulassy, Phys. Rev. Lett. **68**, 1480 (1992)
59. B. Betz, Jet Tomography in Heavy-Ion Collisions - Challenges, Results, and Open Problems, (2022). arXiv:1602.04607 [hep-ph]
60. K. Fukushima, D.E. Kharzeev, H.J. Warringa, Phys. Rev. D **78**, 074033 (2008)
61. O. Rogachevsky, A. Sorin, O. Teryaev, Phys. Rev. C **82**, 054910 (2010)
62. D.E. Kharzeev, D.T. Son, Phys. Rev. Lett. **106**, 062301 (2011)
63. Z. Liang, X.N. Wang, Phys. Rev. Lett. **94**, 102301 (2005)
64. O. Vitiuk, L.V. Bravina, E.E. Zabrodin, Phys. Lett. B **803**, 135298 (2020)
65. S. Mrowczynski, Acta Phys. Polon. B **48**, 707 (2017)
66. K.J. Sun, C.M. Ko, B. Dönigus, Phys. Lett. B **792**, 132–137 (2019)
67. Y. Cai, T.D. Cohen, B.A. Gelman, Y. Yamauchi, Phys. Rev. C **100**, 024911 (2019)
68. J. Aichelin et al., Phys. Rev. C **101**, 044905 (2020)
69. E. Shuryak, J.M. Torres-Rincon, Phys. Rev. C **101**(3), 034914 (2020)
70. D. Oliinychenko, talk given at XXVIIIth Conference Quark Matter 2019. (2022), arXiv:2003.05476v1 [hep-ph]
71. B. Dönigus, Eur. Phys. J. A **56**(11), 280 (2020)
72. O.V. Vitiuk et al., to appear in Euro. Phys. J A. (2022), arXiv:2007.07376 [hep-ph]
73. K.A. Bugaev, Nucl. Phys. A **606**, 559–567 (1996)
74. F. Cooper, G. Frye, Phys. Rev. D **10**, 186 (1974)
75. K.A. Bugaev, Phys. Rev. Lett. **90**, 252301 (2003)
76. K.A. Bugaev, Phys. Rev. C **70**, 034903 (2004)
77. S. Voloshin, Y. Zhang, Z. Phys. C **70**, 665–672 (1996)
78. M. Bleicher et al., (2022), arXiv:1106.3647 [nucl-th]
79. W. Greiner, B. Müller, J. Rafelski, *Quantum Electrodynamics of Strong Fields* (Springer, Berlin, 1985)
80. R.V. Popov et al., Phys. Rev. D **102**, 076005 (2020)
81. V. Voronyuk et al., Phys. Rev. C **83**, 054911 (2011)
82. G.M. Zinovjev, A.M. Snigirev, (2020), https://doi.org/10.3367/UFNe.2020.10.038857